

# Early Dynamical Instabilities in the Giant Planet Systems

E. Lega<sup>1</sup>, \*, A. Morbidelli<sup>1</sup> and D. Nesvorný<sup>2</sup>

<sup>1</sup> *Université de Nice Sophia Antipolis, CNRS UMR 7293, Observatoire de la Côte d’Azur, Bv. de l’Observatoire, B.P. 4229, 06304 Nice cedex 4, France.*

<sup>2</sup> *Southwest Research Institute, Department of Space Studies, 1050 Walnut St., Suite 300, Boulder, Colorado 80302*

Accepted .... Received ....; in original form ....

## ABSTRACT

The observed wide eccentricity distribution of extrasolar giant planets is thought to be the result of dynamical instabilities and gravitational scattering among planets. Previously, it has been assumed that the orbits in giant planet systems become gravitationally unstable after the gas nebula dispersal. It was not well understood, however, how these unstable conditions were established in the first place.

In this work we numerically simulate the evolution of systems of three planets as the planets sequentially grow to Jupiter’s mass, and dynamically interact among themselves and with the gas disk. We use the hydro-dynamical code FARGO that we modified by implementing the  $N$ -body integrator SyMBA. The new code can handle close encounters and collisions between planets. To test their stability, the planetary systems were followed with SyMBA for up to  $10^8$  yr after the gas disk dispersal.

We find that dynamics of the growing planets is complex, because migration and resonances raise their orbital eccentricities, and cause dynamical instabilities when gas is still around. If the dynamical instabilities occur early, planets can be removed by collisions and ejections, and the system rearranges into a new, more stable configuration. In this case, the planetary systems emerging from the gas disks are expected to be stable, and would need to be destabilized by other means (low-mass planets, planetesimal disks, etc.). Alternatively, for the giant planet system to be intrinsically unstable upon the gas disk dispersal, a special timing would be required with the growth of (at least some of) the giant planets having to occur near the end of the gas disk lifetime.

**Key words:** Giant planets dynamics, hydro-codes,  $N$ -body simulations.

## 1 INTRODUCTION

The eccentricity distribution of the extrasolar giant planets is wide with orbits commonly having  $e > 0.3$ . Such a wide distribution was unexpected based on our anticipation from the Solar System

\* E-mail: elena@oca.eu (EL); morby@oca.eu (AM); davidn@boulder.swri.edu (DN)

planets. Different mechanisms have been proposed to explain the high eccentricities values: trapping of planetary pairs in mean motion resonances (Lee and Peale (2002)), the Kozai cycles in binary systems (Mazeh et al. (1997); Holman et al. (1997)), stellar jets (Namouni (2005)), and gravitational scattering during global dynamical instabilities (Weidenschilling and Marzari (1996); Rasio and Ford (1996); Lin and Ida (1997)).

This last mechanism has been investigated with extensive  $N$ -body simulations (Chatterjee et al. (2008); Raymond et al. (2009); Juric and Tremaine (2008)). All these studies assumed that the planetary systems emerging from the gas disks are intrinsically unstable, and the gravitational interactions among planets cause instabilities after the gas disk dispersal. The subsequent scattering encounters between planets lead to large orbital eccentricities, just as needed to explain the observations.

A hydro-dynamical code has been recently used to study the planetary system instabilities in a low-density rapidly-dispersing disk (Moeckel and Armitage (2012)). The initial orbits of the planets were assumed to be circular and close enough to each other to be unstable, without any mutual resonance relationship. It was found that the disk can stabilize some of the planetary systems by driving them into resonance rapidly. However, the systems that became unstable ended up behaving as in the gas-free simulations.

The investigations discussed above, including Moeckel and Armitage (2012), adopt similar choices of initial conditions with unstable and sometimes overlapping planetary orbits. In reality, the initial conditions of these studies should be informed from the previous stages of planet-disk interactions when the damping effects of gas were important.

The orbital dynamics of giant planets in a massive gas disk has been studied with a hydro-dynamical code by Marzari et al. (2010). They started their simulations with the fully-formed giant planets and ignored the previous stage during which the giant planets had grown by gas accretion onto their cores.

Here we report the result of the first effort to investigate the dynamical evolution of planets from their growth phase from cores to aftermath of the gas disk dispersal. Our simulation set up is different from those of previous works and is defined according to the following rationale. Planetary cores are expected to form by oligarchic growth (Kokubo & Ida (1998)) with orbital separations of about 10 mutual Hill radii. However, during and after their formation they migrate in the disc due to their gravitational in-

teractions with the gas. According to the Pollack et al. model (Pollack et al. (1996)) the cores can spend a few millions years in the disc before accreting gas in a runaway fashion and become giant planets. In this time they can substantially modify their orbits and reach a new equilibrium configuration. While it was thought in the past that cores continuously migrate toward the central star (Ward (1997)), it is now known that in a disc with realistic heat diffusion they migrate towards an orbital radius where migration is cancelled (Paardekooper & Mellema (2006); Kley et al. (2009); Lyra, Paardekooper, & Mac Low (2010)). This no-migration radius acts as a *planet trap*. If multiple cores are present they are expected to reach a resonant non migrating configuration near the trap (Morbidelli et al. (2008)). In this configuration the cores can be much closer to each other than their initial 10 Hill radii separation which may lead to very strong instabilities when the planets grow to Jupiter mass.

With this kind of dynamical evolution in mind, in our hydrodynamical simulations we set up a planet trap and let a system of three embryos of 10 Earth masses to evolve until they reach a stable resonant configuration. Then, we track the evolution of the systems as each of the three planets grows in sequence to one Jupiter mass. Finally, we slowly remove the gas from the disc and follow the evolution of the systems up to  $10^8$  years after the gas dispersal. We use the hydro-dynamical code FARGO (Masset (2000)) modified in Morbidelli and Nesvorný (2012) by implementing the  $N$ -body integrator SyMBA (Duncan et al. (1998))<sup>1</sup> to handle close encounters and mutual collisions between planets.

The paper is organized as follows. Section 2 explains the set-up of our numerical simulations. The dynamics of growing planets is described in Section 3. We then discuss the effects of the gas disk dispersal and the subsequent stage of purely  $N$ -body interaction of the remaining planets (Section 4). Conclusions are given in Section 5.

## 2 SETUP OF NUMERICAL SIMULATIONS

### 2.1 Disk parameters

We used the hydro-dynamical two-dimensional code FARGO (Masset (2000)), in which the orig-

<sup>1</sup> We use `swift_symba7` that is capable of correctly handling the closely-packed planetary systems (Levison et al. (2011)).

inal  $N$ -body Runge-Kutta integrator was replaced (Morbidelli and Nesvorny (2012)) with the symplectic integrator SyMBA (Duncan et al. (1998)). The SyMBA code was specifically designed to handle close encounters and mutual collisions between planets. As the hydrodynamical simulations are CPU expensive, we were not able to run many simulations to fully explore parameter space. Instead, we considered a few cases that illustrate different aspects of the problem.

Two different disks were considered (denoted by  $A$  and  $B$  in the following) with the initial mass  $M_A = 0.009M_\odot$  in case A and  $M_B = 0.018M_\odot$  in case B, where  $M_\odot$  is the mass of the Sun. In each case we performed several simulations that differed in the prescription for the growth of the planets (see below).

We use units such that  $G = 1$  and  $M_\odot = 1$ . The orbital period of a planet with semi-major axis  $a = 1$  is therefore  $T = 2\pi$ . We normalize the time  $t$  by  $T$  in the following, so that  $t$  corresponds to the number of orbits at  $a = 1$ , or years. The disk's kinematic viscosity coefficient is set to be  $\nu = 10^{-5}$  in these units. The initial surface density profile scales with the distance  $r$  from the star as  $r^{(-1/2)}$ .

Our computational domain consists of an annulus of the protoplanetary disk extending from  $r_{min}$  to  $r_{max}$ . Different disk extensions have been used in different cases. In some cases (specified below), the disk had to be extended during the simulations when the migration caused the innermost planet to approach the inner boundary. To start with we used  $r_{min} = 0.5$ ,  $r_{max} = 4.5$ , and a grid of  $N_r = 660$  linearly spaced radial cells and  $N_s = 700$  azimuthal cells.

The width of planet's horseshoe region is given, in the isothermal disk approximation (Masset et al. (2006b)), by:

$$x = \sqrt{\frac{(m/M_\odot)}{(H/r)}} a. \quad (1)$$

For example, for a planet of mass  $m/M_\odot = 3 \times 10^{-5}$  (i.e. 10 Earth masses) and disk aspect-ratio  $H/r = 0.05$  we get  $x = 0.0245a$ , where  $a$  is the semi-major axis (see Section 2.2). The radial resolution of 0.006 allows us to resolve the horseshoe region by at least 4 cells for any  $a \geq 1$ .

The planetary contribution to the potential  $\Phi$  acting on the disc is smoothed according to:

$$\Phi = -\frac{Gm}{\sqrt{d^2 + \epsilon^2}} \quad (2)$$

where  $d$  denotes the distance of a disc element to the planet and  $\epsilon$  is the smoothing-length. In our simulations we used  $\epsilon = 0.5R_H$ , where  $R_H$  denotes the Hill radius.

## 2.2 Initial orbits

Three 10-Earth-mass planetary cores were placed into the disk and were initially evolved till they reached a stable configuration in a resonance. We used a planet trap (Masset (2002); Masset et al. (2006); Morbidelli et al. (2008)) to halt the orbital migration of the innermost core.

The planet trap was set as a steep and locally positive surface-density gradient in the disk inside the initial orbital location of the innermost core. It allows the system of three cores to acquire stable, separated and non-migrating orbits. The planet trap is convenient way to mimic the situation in real radiative disks where the non-isothermal effects can change the direction of the type-I migration (Paardekooper & Mellema (2006); Kley et al. (2009)). The migration in the inner part of a real radiative disk can be directed outward, while it remains directed inward in the outer disk. This establishes the existence of a critical radius where migration vanishes. The planetary cores migrating inwards will be collected near this radius as in the case of a planet trap (Lyra, Paardekooper, & Mac Low (2010)).

The planet trap location was set at  $a = 3$  in case A and  $a = 2$  in case B. The local and positive surface-density gradient required to form the planet trap was created by imposing a transition in the viscosity from  $4\nu$  to  $\nu$  over  $\Delta r = 1$  around the trap location (Masset et al. (2006)) The initial orbits of the three cores were chosen near the 5:4 resonant chain in case A (semimajor axes  $a_1 = 3.07$ ,  $a_2 = 3.62$  and  $a_3 = 4.20$ ), and near the 3:2 resonant chain in case B (semimajor axes  $a_1 = 2.1$ ,  $a_2 = 2.77$  and  $a_3 = 3.66$ ). The initial eccentricities were set to zero.

In a first step, we followed the evolution of disk and cores, and waited till the cores arranged themselves in a stable resonant configuration. In case A, the cores 3 and 2 ended up in the 6:5 resonance, and cores 2 and 1 in the 7:6 resonance. In case B, two cores reached a coorbital configuration (1:1 resonance) near the planet trap, and the third one ended up in the 6:5 resonance with the other two. The eccentricities remained small at this stage,  $e \sim 0.01$ - $0.02$ , due to the strong damping of gas, and the orbits remained nearly coplanar.

## 2.3 Mass growth

Once the resonant configuration was achieved, the mass of each core was increased from the initial value ( $m(0) = 3 \times 10^{-5}M_\odot$ ) to one Jupiter mass ( $m_J = 10^{-3}M_\odot$ ) as follows:

$$m(t) = m(0) + (m_J - m(0)) \sin^2\left(\frac{\pi}{2} \frac{(t - t(0))}{\Delta t}\right), \quad (3)$$

where  $t(0)$  was the time when the growth started, and  $\Delta t$  was the growth time interval. Different values of  $t(0)$  were chosen for different planets, so that they grew in sequence. Sometimes, we let the innermost core grow first with the other two growing later. In other cases we opted for growing the middle or outer core first (see Section 3).

We didn't consider gas accretion within the Roche lobe. This is a delicate point which is not well understood yet and which goes beyond the purpose of the present work.

The criterion for collision is that the distance between planets becomes equal or lower to one Jupiter radius.

The timescales for the planetary growth that we adopt ( $\Delta t = 10^3$ ,  $3 \times 10^3$ , and  $4 \times 10^3$ , see table 3.1) are too short to be realistic. These timescales are dictated by our current CPU power (using the parallel FARGO code and 30 CPUs we compute 10 to 100 orbits in 1 hour, depending on the disk parameters). Slower growth rates will be investigated in the future.

When a planet grows to Jupiter mass, it is expected that the planet trap should become ineffective and the planet should start migrating inward. We find this behavior in our simulations.

### 3 DYNAMICS IN THE GAS DISK

Here we discuss the orbital dynamics of growing planets in the full gas disk. Each system is evolved over 20000 to 65000 years after the growth of the last planet. To identify the different settings of our simulations we label them  $A_{i,j,k}$  for case A and  $B_{i,j,k}$  for case B, where indices  $i, j, k \in [1, 3]$  indicate the growth order of the three cores (initially  $a_1 \leq a_2 < a_3$ ). The characteristics of each simulation are reported in Table 3.1.

#### 3.1 Case $A_{2,1,3}$

Figure 1 shows the results of simulation  $A_{2,1,3}$ . We find that when core #2 grows to Jupiter mass it starts migrating inward and scatters the other two cores at  $a > 3$ . We remark that the initial location of the trap is at  $a = 3$ , but the gap opened by core #2 has shifted the trap at  $a = 4$ . Therefore, cores #1 and #3 remain trapped at quasi constant semi-major axis, respectively at  $a \simeq 4$  and  $a \simeq 5.6$  till core #1 grows. As the fully grown planet #1 starts migrating inwards at  $t = 8000$ , it opens a gap and shifts the trap location at  $a \simeq 5.5$ . Core #3 is scattered out and remains near the new trap position at  $a \simeq 5.5$  till  $t_3(0) = 12000$ . Core #3 then starts growing and inward migration begins.

Once all three planets reach Jupiter mass they migrate inward and evolve into mutual resonances. Their orbital eccentricities rapidly grow to large values by resonant interactions. The system becomes highly unstable. The gas density distribution is strongly perturbed at this point (Fig. 2) leading to complex gas-planet interactions. Finally, at  $t = 20000$  years, the inner planet is lost by plunging into the star.

Our criterion for collision with the star is that the pericenter of the planet's orbit becomes smaller than 0.01. The tidal effects are ignored in our simulation. In reality, however, the tidal effects should start to be dominant for small pericenters, potentially leading to the circularization of the orbit in the hot Jupiter region (Beauge & Nesvorný (2012)). This effect would result in decoupling the planet from the other two. So, in any case, the inner planet's influence on the other two is suppressed. The subsequent evolution of the two-planet system leads to stable orbits with moderate eccentricities.

#### 3.2 Case $A_{3,1,2}$

In our first simulation core #3 was grown on  $\Delta t = 10^3$ . One of the two remaining cores was ejected from the system during the growth of core #3. We have therefore reconsidered this case with a longer phase of growth of core #3,  $\Delta t_3 = 4 \times 10^3$  (table 3.1). In this case, the transition is less violent, core #2 is scattered out and its semi-major axis remains stable at the new trap location (after gap opening by planet #3), i.e. at  $a \simeq 4.3$ . Core #1 migrates inward at the same rate as the fully grown planet #3 (Fig. 3). The growth of core #1 then leads to a phase when the other two planets are scattered outward. The subsequent dynamics is complex with episodes of outward migration, and a rapid increase of the eccentricities after the growth of planet #2. As in case  $A_{2,1,3}$ , the system becomes highly unstable. Planet #1 is then ejected from the system. These early ejections could be related to free-floating planets (Sumi et al. (2011)).

The orbits of the remaining two planets are chaotic till  $t = 52594$ , when the two planets merge.<sup>2</sup> The remaining giant planets migrates inward and converges to a circular orbit.

<sup>2</sup> Note that merging events may happen too often in our simulations due to the coplanar approximation of the system.

Simulation	$[r_{min}, r_{max}]$	$\Delta t$	$(N_r, N_s)$
$A_{2,1,3}$	[0.5, 6.5]	$10^3$	(660,700)
$A_{3,1,2}$	[0.5, 9.5]	$\Delta t_3 = 4 \times 10^3$	(660,700)
		$\Delta t_{1,2} = 10^3$	
$A_{3,2,1}$	[1, 9.5]	$3 \times 10^3$	(660,700)
	[0.5, 9.5] $t \geq 20000$		(700,700)
$B_{1,2,3}$	[0.5, 4.5]	$10^3$	(660,700)
	[0.1, 4.5] $t \geq 8500$		(720,700)
$B_{3,1,2}$	[0.5, 4.5]	$10^3$	(660,700)
	[0.1, 4.5] $t \geq 8500$		(720,700)
	[0.3, 4.5] $t \geq 30000$		(690,700)

**Table 1.** Simulations parameters.

### 3.3 Case $A_{3,2,1}$

In case  $A_{3,2,1}$ , all the three cores grow on  $\Delta t = 3 \times 10^3$  (Fig. 4). The growth phase leads to the inward migration of the growing planet #3. The other two cores are scattered outward. The subsequent phase is quite different with respect to the two previous cases. Here the system settles in a stable resonant 2:1 configuration with planets slowly migrating inward, and eccentricities reaching moderate values ( $e \sim 0.2-0.3$ ).

We remark that three of the four planets found around the red dwarf Gliese 876 are on the triple 2:1 resonant configuration (Rivera et al. (2010)). The masses of the planets as well as their distance from the star are different from our simulation so that our comparison is only qualitative but nevertheless interesting.

To avoid spurious boundary effects, the disk was extended to  $r_{min} = 0.5$  at  $t = 20000$ , when the pericenter of planet #3 was close to 1. The radial density profile has been extrapolated from the inner disk edge, and the simulation restarted with the extended disk.

### 3.4 Case $B_{1,2,3}$

In this case, cores #1 and #2 become coorbital at the trap location. It is interesting that they remain coorbital during the growth phase even if they do not grow at the same time (see Fig. 5). The third core is scattered out when planet #1 grows. It then migrates inward until it reaches the trap at  $a \simeq 2$ . When its mass starts increasing, #3 migrates inwards, and all three planets reach in a compact orbital configuration. The disk has been extended to  $r_{min} = 0.1$  at  $t = 8500$  using the same procedure as for case  $A_{3,2,1}$ . The extended disk is followed with a time-step of  $\simeq 10^{-3}$ . To calculate 10 orbits this requires about 1 hour on 30 CPUs. The two coor-

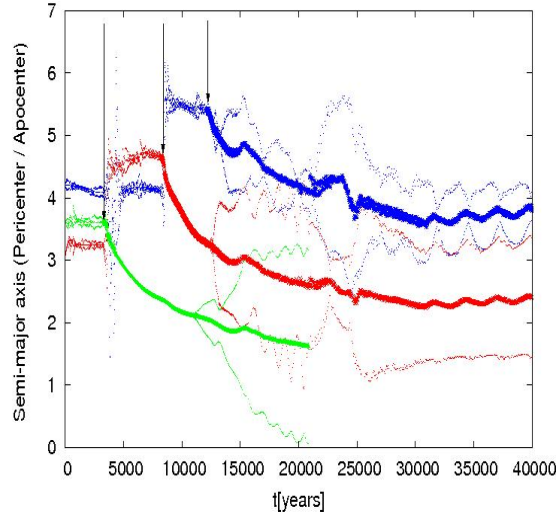


**Figure 1.** Dynamical evolution of the planets in simulation  $A_{2,1,3}$ . Each planet is represented by different color: red for planet #1 (initially the innermost one); green for planet #2 (middle); blue for planet #3 (outermost). For each planet the three curves denote the pericenter, semimajor axis and apocenter as a function of time. The masses of the cores grow to Jupiter mass according to Eq. 3 on  $\Delta t = 1000$  starting  $t_2(0) = 3200$ ,  $t_1(0) = 8000$  and  $t_3(0) = 12000$ . The arrows highlight  $t(0)$  for each planet.

bital planets merge at  $t = 13275$  and the third one is scattered out. The eccentricities of the two remaining planets grow to moderate values. The planets end up in the 3:1 resonance.

### 3.5 Case $B_{3,1,2}$

Core #3 grows first and scatters two coorbital cores outward. The two cores appear to be on the trap at very small angular separation  $\Delta\alpha$  with:  $10^\circ < \Delta\alpha < 30^\circ$ . It is therefore possible

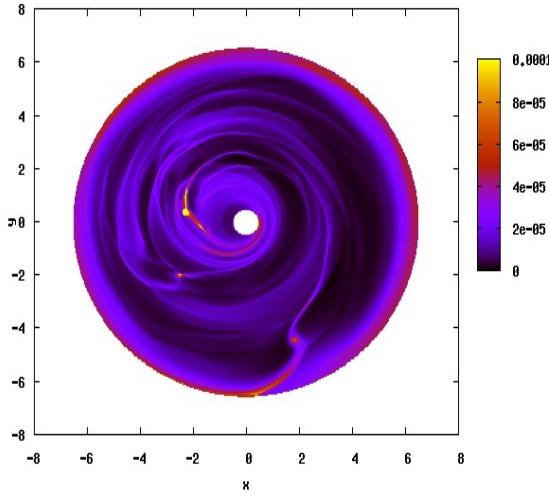


**Figure 2.** Gas surface density in the simulation shown in Fig. 1 at  $t = 15000$ . Three eccentric Jupiter-mass planets produce a complex distribution of gas. Color scale range was chosen such that dark blue corresponds to values  $\leq 10^{-5}$  and yellow to values  $\geq 10^{-4}$  (in dimensionless units).

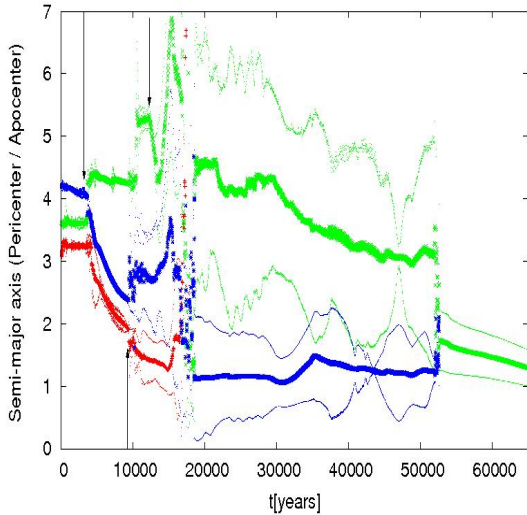


**Figure 3.** The same as Fig. 1 for case  $A_{3,1,2}$ . The arrows highlight the  $t(0)$  values:  $t_3(0) = 3200$ ,  $t_1(0) = 8700$  and  $t_2(0) = 12000$ .

that the scattering event affect them on the same way. Actually, as a result of the scattering they remain coorbital and only their angular separation changes drastically. The two orbits separate at  $t = 7000$  when core #1 starts growing. Once that happens, core #1 scatters the core #2 out-

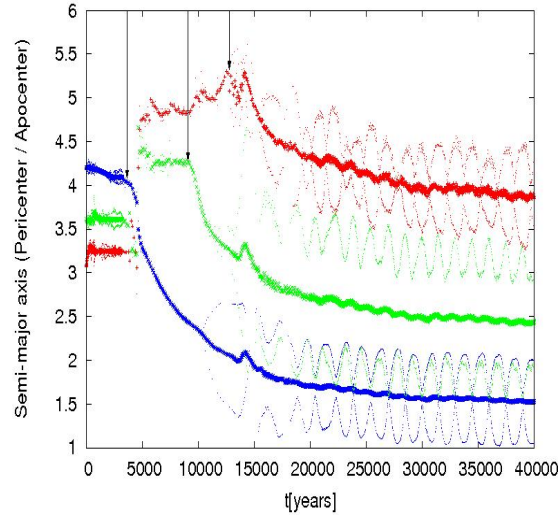


**Figure 4.** The same as Fig. 1 for case  $A_{3,2,1}$ . The growth of cores started at  $t_3(0) = 3200$ ,  $t_2(0) = 8600$  and  $t_1(0) = 12000$ , as indicated by the arrows.

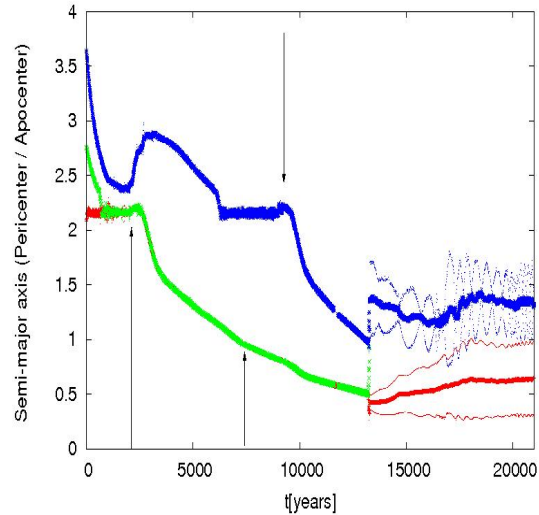


**Figure 5.** The same as Fig. 1 for case  $B_{1,2,3}$ . The growth of cores started at  $t_1(0) = 2000$ ,  $t_2(0) = 7000$  and  $t_3(0) = 9000$ , as indicated by the arrows.

ward (Fig. 6). After the growth of core #2, a complex instability arises resulting in the ejection of #3 from the system. The two remaining planets have moderate eccentricities and persist on chaotic orbits showing an outward migration trend till  $t = 33900$  when the two planets merge. This case is comparable to case  $A_{3,1,2}$ .

The disk has been extended to  $r_{min} = 0.1$  at  $t = 8500$ . In order to follow the chaotic evolution of the two planets on reasonable CPU times, we

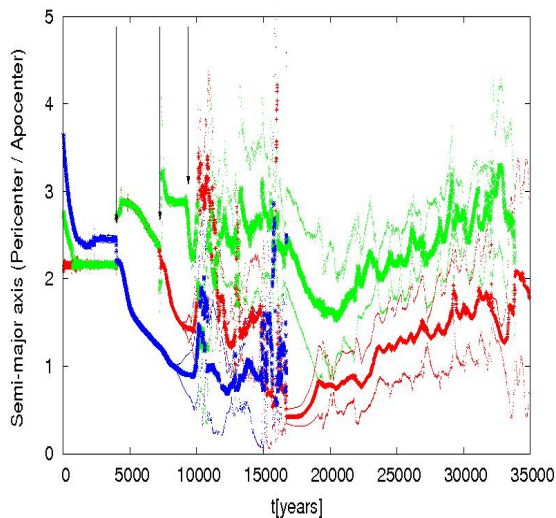


**Figure 6.** The same as Fig. 1 for case case  $B_{3,1,2}$ . The growth of cores started at  $t_3(0) = 3700$ ,  $t_1(0) = 7000$  and  $t_2(0) = 9000$ , as indicated by the arrows.

have then reduced the disk domain increasing  $r_{min}$  to 0.3 at  $t = 30000$ .

### 3.6 Summary

From the limited number of cases that we have investigated so far, we can derive the following tentative implications for the dynamics of systems with three giant planets and their interaction with a gas disk:

(i) If the gas lasts long enough after the growth of the last giant planet, the system develops an instability and one planet is typically lost. These ejections could be related to free-floating planets (Sumi et al. (2011)).

Indeed, only in one case out of five we obtained a final stable system with three giant planets. This is at odds with the results of Matsumura et al. (2010) who found that the three-planet systems often survive to the end of gas disk lifetime. This difference may appear from the approximate treatment of the gas disk in Matsumura et al. (2010). When the gas density is strongly perturbed as in Fig. 2 it acts as an additional source of stochasticity in the planetary evolution. Marzari et al. (2010), who used a hydrodynamical code similar to ours, also found that systems of fully-grown giant planets on close orbits *rarely* survive to the end gas disk lifetime.

(ii) The simplified two-planet systems, that emerge from the three-planet systems when the the third planet is eliminated, tend to be stabilized by their interaction with the gas disk. This was also pointed out in Marzari et al. (2010);

Matsumura et al. (2010) and in Moeckel, Raymond, & Armitage (2008). In some cases, the two-planet system shows chaotic evolution till the system is reduced by a merging event. Future work on the full spatial problem will be needed to better explore the frequency of merging events.

(iii) We did not find any case where the giant planets would end up on nearly-circular closely-packed orbits. This raises doubts about the applicability of the initial conditions used in the models of planet scattering after the gas disk dispersal (see Section 1; Chatterjee et al. (2008); Raymond et al. (2009); Juric and Tremaine (2008)).

## 4 GAS DISPERSAL AND GAS-FREE DYNAMICS

In the previous section we assumed that the gas disk remains present after the accretion of the giant planets, that is until the planets reach a stable dynamical configuration. It is possible, however, that the gas dispersal occurred *during* the planetary instability or soon after it, such that the planetary system did not have enough time to fully stabilize. Here we investigate these cases.

The gas density was reduced at each time step  $dt$  as:

$$\rho' = \rho \left(1 - \frac{dt}{\tau}\right), \quad (4)$$

where the coefficient  $\tau \simeq 2000$  years. This dissipation timescale is very short when compared to the  $10^5$  years timescale considered for photoevaporation in Matsumura et al. (2010). We find that, if the gas is removed too fast, planetary systems can become unstable. In our simulations, we didn't observe any scattering events or merging during the dissipation phase, so that we are confident that our results wouldn't change much using a longer dissipation timescale.

We recall that our purpose is not to quantitatively describe a specific phase of the giant-planet-disk interaction but to obtain a qualitative description of the whole phenomenon; this justify also the use of a dissipation function (4) which is simple with respect to the description in Moeckel and Armitage (2012).

When the disk gas density drops to values below  $\sim 10^{-10}$  (in dimensionless units), the effect of gas becomes negligible and we continue the integration with SyMBA (Duncan et al. (1998)). The planetary systems are evolved for up to  $10^8$  years.

We first tried a case where gas was removed after the planetary system has reached its final configuration. Fig. 7 shows the orbits for case  $A_{2,1,3}$ , where the gas disk was removed in the

time interval [35000, 37000]. During the removal, planetary migration slows down and the two remaining planets stay in the 2:1 resonance for the whole  $N$ -body integration. The same applies to  $B_{1,2,3}$ , where no scattering event was found after the gas dispersal (gas was removed at [19000, 20000] in this case).

In  $A_{3,2,1}$ , where three planets initially survived, they also survived for the whole length of the  $N$ -body integration. The three planets remained in the 2:1 resonant chain and no scattering among them occurred (Fig. 8). This happened independently of the removal time (if chosen after  $t = 20000$  years in Fig. 4) and independently of the removal timescale  $\tau$ .

In Matsumura et al. (2010), in agreement with our results, the two-planet systems also remained stable. For the three-planet systems, Matsumura et al. (2010) found stability (e.g., see their Fig. 4) only in some cases. Unfortunately, having only one three-planet system we cannot test the statistical significance of our result. Note also that the previous versions of the SyMBA code used in Matsumura et al. (2010) had a later-identified problem when tracking closely-packed planetary systems (Levison et al. 2011). It has to be verified that this problem did not cause artificial instabilities in some of their integrations.

We now turn our attention to the possibility that the gas disk dispersed during the planetary-scattering phase. In Fig. 9, we removed gas in the interval [15000, 17000] during the evolution of system  $A_{2,1,3}$  (Fig. 1). In this case, the three giant planets undergo a gravitational scattering event in which one planet is ejected and the remaining two are sent onto highly-eccentric mutually-decoupled orbits (Fig. 9). The same kind of evolution happened in all cases investigated here, provided that the gas disk was removed during the scattering phase.

## 5 CONCLUSIONS

We used a hydro-dynamical code to follow the orbital evolution of systems of three planets as they grew in sequence to Jupiter mass. We found that the planet system changes drastically after the growth of each core. The orbital evolution of planets can be very complex. More often than not the orbits become unstable leading to a phase of planetary scattering. Planets can be ejected or merge (Marzari et al. (2010)).

Once the system is reduced to two planets the dissipative effects of gas decrease orbital eccentricities of the remaining planets, and migrate planets into a new, stable resonant configuration. In only one case out of five, there was no in-

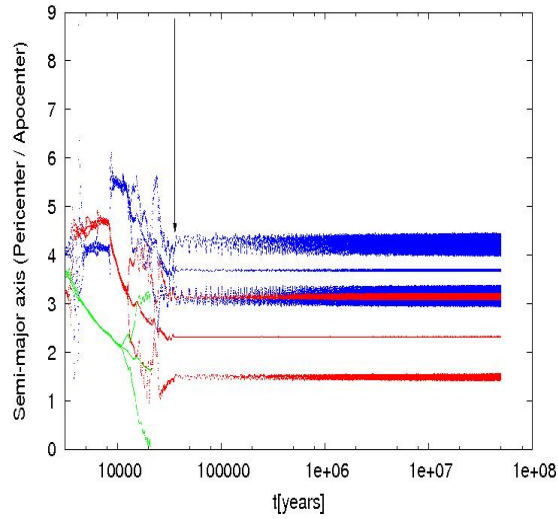


**Figure 7.** Evolution of planetary orbits in case  $A_{2,1,3}$ . The gas disk is removed at [35000, 37000], and an  $N$ -body integrator is used to follow the gravitational interactions among planets for  $t > 37000$ . The arrow indicates the beginning of the gas-free phase.

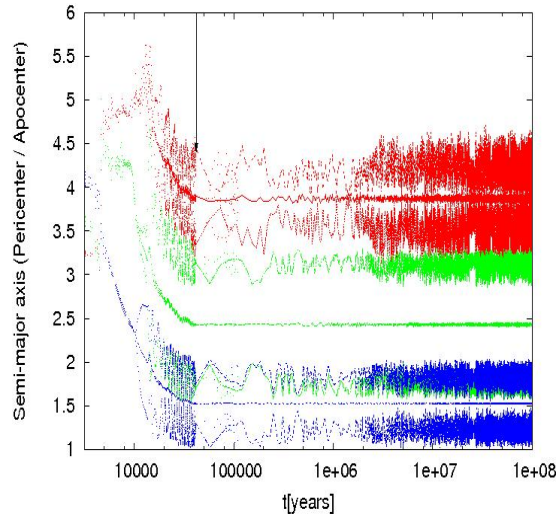


**Figure 8.** Evolution of planetary orbits in case  $A_{3,2,1}$ . The gas disk is removed at [39500, 41000]. The arrow indicates the beginning of the gas-free phase.

stability happening after the growth of all three planets. The three-planet system remained in a resonant stable configuration in this case.

If the gas disk is removed after the new stable configuration is achieved, the orbital eccentricities remain low and the system is stable. This is at odds with the assumption typically made in the planet-scattering models (Chatterjee et al. (2008); Raymond et al. (2009); Juric and Tremaine (2008)), where gas is ignored and



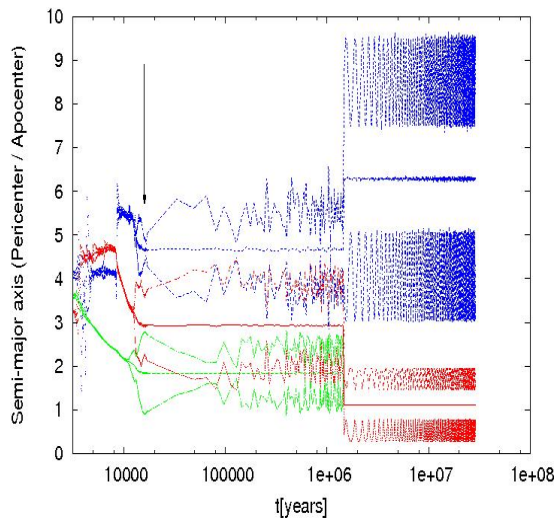


**Figure 9.** Evolution of planetary orbits in case  $A_{2,1,3}$ . The gas disk is removed at [15000, 17000]. The arrow indicates the beginning of the gas-free phase.

the planets are initially placed on closely-packed unstable orbits. Here we show that these initial conditions may not naturally arise from a previous stage, in which the planets interacted with their natal protoplanetary disk.

If the gas disk is removed during the planetary instability, planetary scattering continues after the gas removal and the surviving planets can reach very eccentric orbits. However, given the short duration of the planetary instability phase, the removal of gas during this phase would require special timing. For example, it may be possible that the giant planets generally form toward the end of the disk lifetime. Or, as long as there is gas in the system, the existing giant planets keep growing and new giant planets keep forming. This would lead to a richer sequence of planetary instabilities than the one investigated here. We will investigate this possibility in the future work.

Another possibility is that the number of giant planets that form in a typical disk is large ( $> 3$ ). The  $N$ -body simulations have already shown that the eccentricity distribution of exoplanets implies that at least three giant planet existed in a typical system after the gas disk dispersal. Our results seem to suggest that, for this condition to be fulfilled, more than three planets have to form originally.

Alternatively, the giant-planet systems that emerge from gas disks are stable in isolation, as suggested by in the simulations performed in this work, but become unstable due to external causes (interactions with smaller planets, effects

of the planetesimal disks, etc.; e.g. Tsiganis et al. 2005, Levison et al. (2011)).

In conclusion, the results presented here show that the problem of understanding the dynamical paths leading to the surprisingly large eccentricities of extrasolar planets is not fully resolved. Future work should improve upon our efforts by using more realistic prescriptions for the planet growth and gas dispersal, extend the simulation to longer timescales, and perform a larger number of simulations so that the statistical significance of individual outcomes and their dependence on disk parameters is better understood.

## ACKNOWLEDGMENTS

The computations have been done on the “Mesocentre SIGAMM” machine, hosted by the Observatoire de la Cote d’Azur. D.N. acknowledges support from the NSF AAG program.

## REFERENCES

- Beaugé C., Nesvorný D., *ApJ*, 763, 12 2013.
- Chatterjee, S., Ford E.B., Matsumura, S. and Rasio, F.A. Dynamical outcomes of planet-planet scattering. *Ap. J.*, 658:580-602, 2008.
- Duncan, M. J., Levison, H. F. and Lee, M. H. A Multiple Time Step Symplectic Algorithm for Integrating Close Encounters. *Astron. J.*, 116:2067-2077, 1998.
- Juríc M. and Tremaine, S. Dynamical Origin of Extrasolar Planet Eccentricity Distribution. *Ap. J.*, 686:603-620, 2008.
- Holman, M., Touma, J. and Tremaine, S. Chaotic variations in the eccentricity of the planet orbiting 16 Cygni B. *Nature*, 386:254-256, 1997.
- Kley, W., Bitsch, B. and Klahr H. Planet Migration in three-dimensional radiative discs. *A&A*, 506: 971-997, 2009.
- Kokubo E., Ida S., 1998, *Icar*, 131, 171.
- Lee, M.H. and Peale, S.J. Dynamics and Origin of the 2:1 Orbital Resonances of the GJ 876 Planets. *Ap. J.*, 567:596-609, 2002.
- Lin, D.N.C. and Ida, S. On the origin of massive eccentric planets. *Ap. J.*, 477:781-791, 1997.
- Lyra W., Paardekooper S.-J., Mac Low M.-M., Orbital Migration of Low-mass Planets in Evolutionary Radiative Models: Avoiding Catastrophic Infall. *ApJ*, 715, L68, 2010
- Levison H. F., Morbidelli A., Tsiganis K., Nesvorný D., Gomes R. Late Orbital Instabilities in the Outer Planets Induced by Interaction with a Self-gravitating Planetesimal Disk. *AJ*, 142, 152, 2011

- Marzari, F., Baruteau, C. and Scholl, H. Planet–planet scattering in circumstellar gas disks. *A & A* 514, L4, 2010.
- Masset, F.S. FARGO: A fast Eulerian transport algorithm for differentially rotating disks. *Astron. Astrophys. Suppl. Series*, 141:165-173, 2000.
- Masset, F.S. The co-orbital torque in a viscous disk: Numerical simulations. *A& A*, 387:605-623, 2002.
- Masset, F.S., D’Angelo G. and Kley W. On the Migration of Protogiant Solid Cores. *Ap. J.* 652: 730-742, 2006b.
- Masset, F.S., Morbidelli A., Crida, A. and Ferreira, J. Disk Surface Density Transitions as Protoplanet Traps. *Ap. J.*, 642: 478-487, 2006.
- Matsumura, S. Thommes, E.W., Chatterjee S. and Rasio, F. Unstable planetary systems emerging out of gas disks. *Ap. J.*, 714:194-206, 2010
- Mazeh, T., Krymolowsky, Y. and Rosenfeld, G. The High Eccentricity of the Planet Orbiting 16 Cygni B. *Ap. J.*, 477, L103, 1997.
- Moeckel N., Raymond S. N., Armitage P. J., Extrasolar Planet Eccentricities from Scattering in the Presence Of Residual Gas Disks. *ApJ*, 688, 1361, 2008.
- Moeckel, N. and Armitage P.J. Hydrodynamic outcomes of planet scattering in transitional discs. *M.N.R.A.S.*, 419:366-376, 2012.
- Morbidelli, A., Crida A., Masset, F. and Nelson, R.P. Building giant-planet cores at a planet trap. *A&A*, 478:929-937, 2008.
- Morbidelli A., Nesvorný D., 2012, *A&A*, 546, A18, 2012.
- Namouni, F. On the Origin of the Eccentricities of Extrasolar Planets. *Astron. J.*, 130:280-294, 2005.
- Paardekooper S.-J., Mellema G., Halting type I planet migration in non-isothermal disks *A&A*, 459, L17, 2006
- Pollack J. B., Hubickyj O., Bodenheimer P., Lissauer J. J., Podolak M., Greenzweig Y., 1996, *Icar*, 124, 62
- Rasio, F.A. and Ford, E.B. Dynamical Instabilities and the Formation of Extrasolar Planetary Systems. *Science*, 274:954-956, 1996
- Raymond S. N., Barnes R., Veras D., Armitage P. J., Gorelick N., Greenberg R., 2009, *ApJ*, 696, L98
- Rivera E. J., Laughlin G., Butler R. P., Vogt S. S., Haghighipour N., Meschiari S. The Lick-Carnegie Exoplanet Survey: A Uranus-mass Fourth Planet for GJ 876 in an Extrasolar Laplace Configuration. *The Astrophysical Journal* 719, 890, 2010.
- Sumi, T.; Kamiya, K.; Bennett, D. P.; Bond, I. A.; Abe, F.; Botzler, C. S.; Fukui, A.; Furusawa, K.; Hearnshaw, J. B.; Itow, Y.; and 29 coauthors Unbound or distant planetary mass population detected by gravitational microlensing, *Nature*, 473, 349, 2011.
- Ward W. R., 1997, *Icar*, 126, 261
- Weidenshilling S.J. and Marzari F. Gravitational scattering as possible origin for giant planets at small stellar distances. *Nature*, 346:619-621, 1996.